CHAPTER 4

Photocatalytic activity of MoS_2, WS_2 and ternary compound MoW-disulfide NPs

4 Photocatalytic activity of MoS_2, WS_2 and ternary compound MoW-disulfide NPs

The photocatalytic activity of the three prepared samples, namely MoS_2, WS_2 and compound MoW-disulfide1 NPs, were studied under the influence of light emitted by a Xenon arc lamp (Xenon Lamp Zolix SLH- X500 Xenon Arc Light Source which provides UV to visible light). The output power of the lamp was 500W and output intensity was 12000lux when measured at a distance of 8cm from the source light. In the photocatalytic activity measurement, we studied the degradation of the maximum intensity peak of the UV-vis spectra under the catalytic process and this peak was monitored with the help of UV-vis spectrometer.

The main reason for the study of the photocatalytic behaviour of the as-synthesized materials is that the materials possess some properties which are very supportive of photocatalytic behaviour. These are as follows.

1. Firstly, all the as-prepared materials are SCs. These have finite energy BG and from the study of PL spectra and KM plot obtained from diffused reflection spectra these materials behave as direct BG materials. Thus they should absorb light energy efficiently and generate electron-hole (e^--h^+) pairs. UV-vis absorption spectra also show good light absorption capacity of the samples. Also, since the materials are found to have MBG in the visible light range, so these could absorb photons having a broad range of energy more effectively.
2. Secondly, the dimension of the materials is in nanoscale. This nanoscale dimension provides a large surface area which is a very important factor for photocatalysis.
3. Thirdly, since the synthesized NPs are in a solid state there is the possibility of they being reusable as a catalyst which could make the photocatalytic process cost-effective.

These are the main features for which we opted to study the photocatalytic behaviour of the as-synthesized nanoparticles.

4.1 Measurement of BET surface area and BHJ pore size distribution of the as-synthesized MoS_2, WS_2 and MoW-disulfide1 NPs using N_2 adsorption-desorption isotherm analyses

Photocatalysis is a light-induced catalytic process. There are mainly two types of photocatalysis based on the phases of reactant and catalyst. These are

1. Homogeneous photocatalysis in which the reactant and catalyst are in the same phase and
2. Heterogeneous photocatalysis in which the reactant and catalyst are in different phase.

In our case, the catalytic process is heterogeneous since the catalysts are solid SCs. In the heterogeneous photocatalytic reaction, the surface area of the catalyst is a very important factor which defines the ease of reaction mechanism. The more is the surface area of catalyst the more is the number of catalyst molecules or atoms which are exposed to light radiation and hence more photoexcitons are generated. In order to study the nature of the catalyst surface, we have analyzed the BET adsorption/desorption isotherm of the three mentioned samples in this section.

The BJH pore size distributions along with the N_2 adsorption/desorption isotherm for each sample are shown in figure 4.1. The shapes of the plots are similar to that which belongs to IUPAC type IV isotherm and indicate that all the materials have mesoporous structure i.e the pores of the material surface are of a size ranging from 2nm to 50nm [1]. The experimentally calculated surface area and pore size for all samples are tabulated in table 4.1. From this table, we have observed that the BET surface area is maximum for the compound MoW-disulfide1 catalysts as compared to that of the other two samples. Also observing the BJH pore size distribution plots we have concluded that the compound NPs catalyst has larger pores than MoS_2 and WS_2 NPs samples.

Since W atoms are larger in size than Mo atoms they introduce some defects, by forming bonds with S atoms in the structure for stabilization of energy, which in turn possibly create some dangling bonds and voids in the lattice of the MoW-disulfide1 compound. A visual diagram of this effect is shown in figure 4.2. This kind of empty space makes the structure more porous as compared to bare MoS_2 and WS_2 and also the size mismatch of W and Mo leads to larger pore size in the compound catalyst. The larger value of the surface area in the ternary compound material is probably due to the larger pores

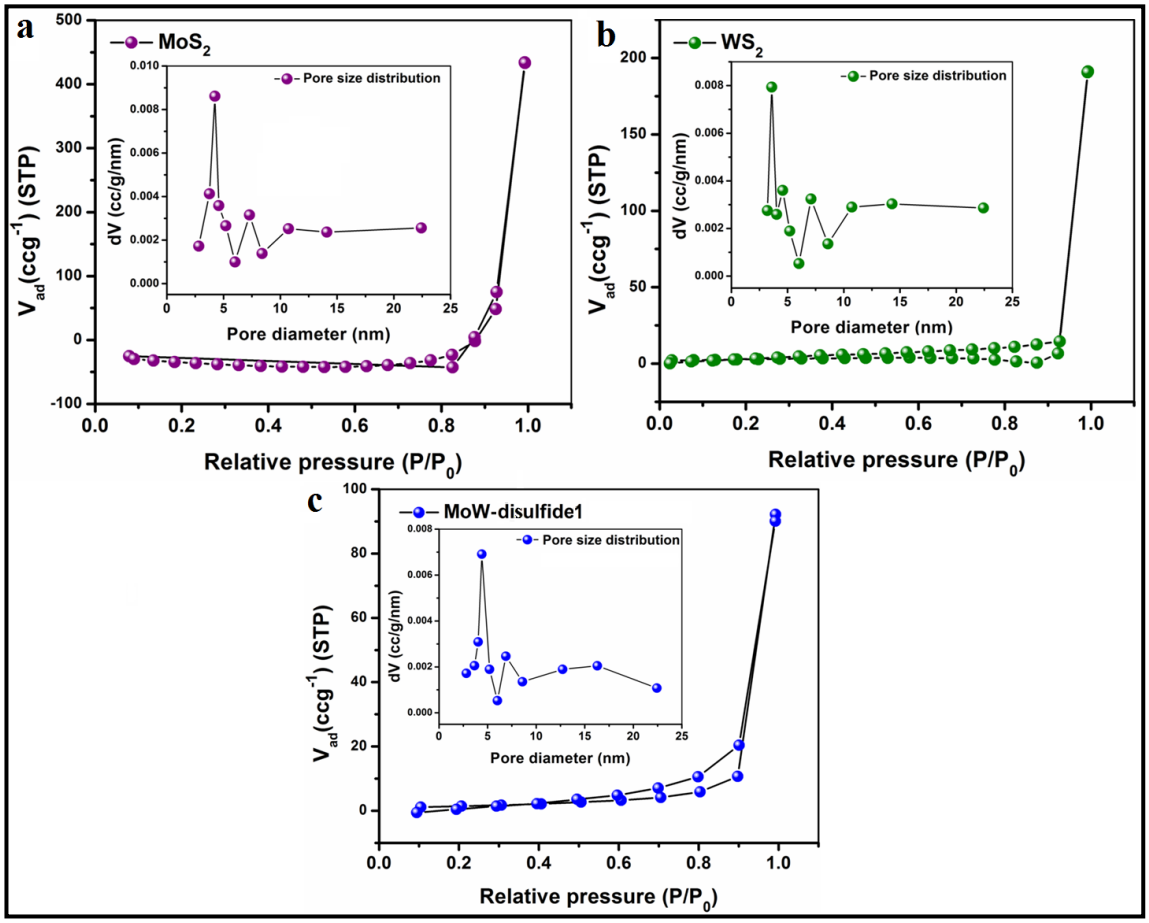

Figure 4.1 N_2 adsorption/desorption isotherm and the BJH pore size distribution (inset) of (a) MoS_2, (b) WS_2 and (c) MoW-disulfide1 NPs as photocatalysts.

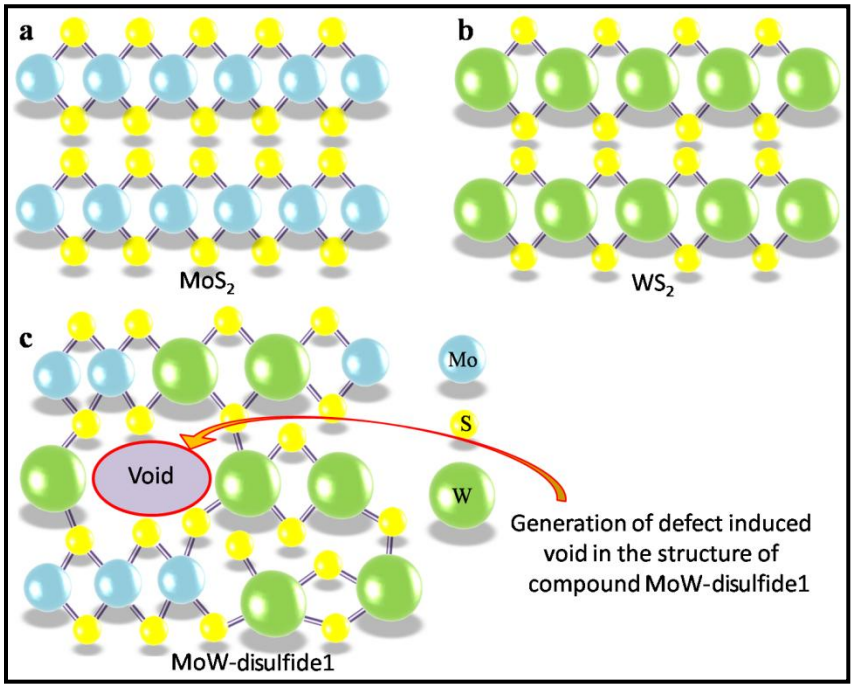

Figure 4.2 (a) and (b) represent MoS_2 and WS_2 system respectively having no defect states. (c) a schematic of the generation of lattice vacancy due to the size mismatch of W and Mo in the ternary compound system.

which effectively increase the surface area [2].

Table 4.1 BET surface area and BJH pore size values of the as-synthesized catalysts.

Sample	MoS_2	MoW-disulfide1	WS_2
BET surface area (m^2/g)	11.67	12.45	9.86
Pore size (Å)	19.84	22.13	17.95

4.2 Determination of optical energy BG values from KM plot

Being heterogeneous photocatalysts the as-synthesized materials should have finite energy BG values so that they can absorb light radiation efficiently. We obtained optical energy BG values by using KM plot from the UV-vis diffuse reflection spectra of the three materials which were discussed in chapter 3. The KM function F(R) and KM equation are given in equations 3.3 and 3.4 respectively in chapter 3 [3]. Here we have replotted the graphs and shown in figure 4.3. We have observed MBG values for each sample and the BG values are tabulated in table 4.2. The BG values confirm that the materials are SC in nature. Mixed-phase polycrystalline nature of the materials and defect states possibly provide MBGs, the energy of which lie in the visible light spectra.

Table 4.2 Optical energy BG values of all the as-prepared catalyst.

Sample	MoS_2	MoW-disulfide1	WS_2
BG (eV)	1.56, 2.76	1.65, 2.41, 2.84	1.58, 2.74

It has been observed in figure 4.3(b) that the compound MoW-disulfide1 NP catalyst exhibits higher values of BG than MoS_2 and WS_2 NPs and the BG energy values lie in the intense part of the solar spectra in near blue light range. The combined effect of ligand S with W and Mo atoms in the ternary compound structure leads to spin splitted d-orbitals that raise the energy levels which in turn increases the BG corresponding to a energy required for absorption of the most intense part of the solar spectrum having larger photon density [4, 5]. The MBGs, occurring due to the presence of mixed phases of the material, provide a better way to utilize a broad spectrum of the solar radiation during photocatalysis and generating more number of e^- - h^+ exciton pairs that hasten the reaction mechanism. Also, the presence of Mo and W in the ternary compound gives rise to more number of dangling bonds as compared to bare MoS_2 and WS_2. This provides generation of more exciton pairs in the compound material in an easier way than in case of bare MoS_2 and WS_2. Also, it has been reported that for SC nanocrystals, as in our case, the generation of

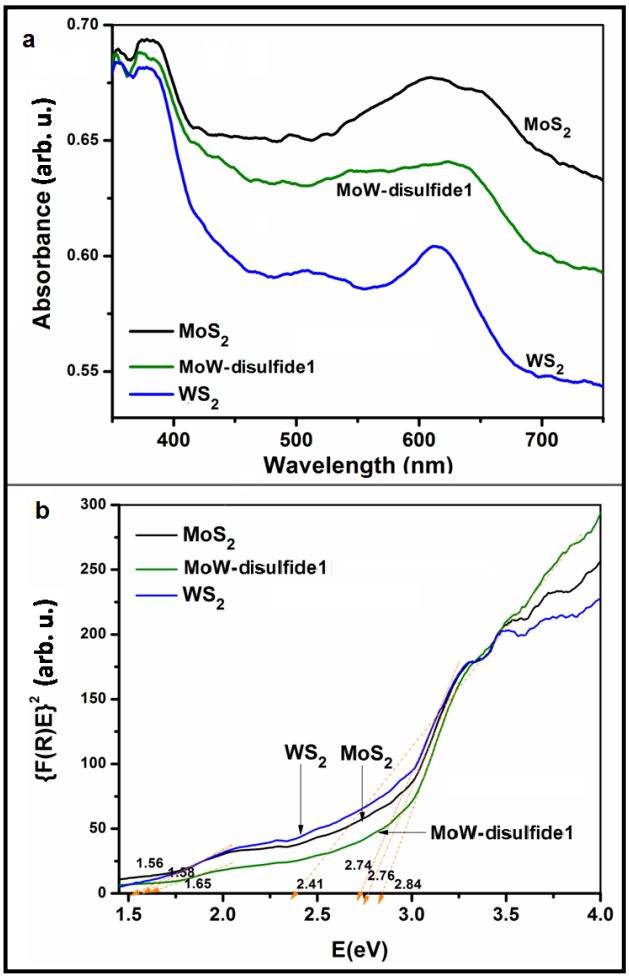

Figure 4.3 (a) The UV-vis spectra and (b) KM plot showing different values of optical BGs of all the as-prepared catalysts.

multiple exciton pairs from a single photon becomes very efficient [6]. These are the important factors for which the compound material shows enhanced photocatalytic activity as compared to MoS_2 and WS_2 which is discussed in the following sections.

4.3 Process of photocatalytic activity

The photocatalytic behavior of the as-prepared materials was evaluated by using MO and RB as model dyes. For this purpose, we prepared a 10μM solution of each dye. The catalyst material was then added to the solution in the amount 1mg/ml and subjected to stirring for several hours in the dark so that absorption-desorption equilibrium was attained. Then the stirred mixture was kept 8cm below the source light and exposed to radiation. 10ml of the solution was taken out at an interval of 30minutes in the absence of light. These samples were then centrifuged at 7000rpm so that the catalyst particles were separated from the dye solution. 3ml of the aliquot was taken from each sample for further analyses to study the UV-Vis absorption behavior. In our photocatalytic experiment, the system allowed air circulation which provided required dissolved oxygen for the catalytic reaction.

4.3.1 Evaluation of photocatalytic activity

The photocatalytic activities of the as-synthesized materials were evaluated by observing the degradation of maximum intensity peak in the UV-vis spectra of model dyes such as MO and RB. The UV-vis absorption spectra of MO and RB under the catalytic influence of MoS_2, MoW-disulfide1 and WS_2 NPs as catalyst are shown in figure 4.4. In the spectra, the maximum absorption for MO is observed at wavelength 463nm while for RB it is observed at 454nm. As seen in figure 4.4(a-c) the absorption of light by MO solution occurs in the range from 350nm to 550nm and in figure 4.4(d-f) we have observed that RB absorbs light in the range 450nm to 600nm. From the spectra in figure 4.4 the decrease in absorption peak with increasing irradiation time in presence of catalysts, which is in agreement with our assumption, is clearly ascertained for both dyes. Both dyes are degraded by the influence of our as-synthesized catalyst under the radiation exposure. Using equation 4.1 (mentioned as equation 2.13 in Chapter 2) the percentage degradation of absorption peaks for the catalytic processes are determined [7, 8].

$$\% D = \left\{ (A_0 - A_t) \Big/ A_0 \right\} \times 100\% \qquad (4.1)$$

where A_0 and A_t are the initial absorbance and absorbance after exposure to light for time t. In figure 4.5(a, b) we have plotted the %D versus time of light exposure (t) for MO and RB using the three different catalysts. From figure 4.5(a & b) it is observed that MoW-disulfide1 compound material exhibits higher degradation efficiency than MoS_2 and WS_2. The compound catalyst degrades both dyes by approximately 98%-99% in just 90 minutes showing better degradation than shown by catalyst MoS_2 and WS_2 NPs. Also, we have observed no degradation of the dyes MO and RB in the absence of any catalyst under light exposure as shown in figure 4.5(a & b). Figure 4.5(c & d) shows the decolorization of MO and RB respectively using MoW-disulfide1 NPs as a catalyst. As observed in BET absorption-desorption isotherm analysis, the larger surface area in case of compound MoW-disulfide1 catalyst provides more space for light to interact with more number of catalyst molecules which generate a larger number of exciton pairs. Also, the mixed phase and defect states in the nanomaterial lower the recombination rate of the photogenerated exciton pairs which also enhances the photocatalytic activity of the compound catalyst [9-11].

The photocatalytic mechanism can be understood from the schematic in figure 4.6. The photogenerated exciton pairs, before they recombine, react with water and oxygen molecule absorbed in water to produce hyper-reactive hydroxyl (•OH) and superoxide anion($\bullet O_2^-$) groups. The hyper-reactive hydroxyl free radicals, superoxide anions, and photo-generated holes further react with the target dye molecules and degrade them making the catalytic reaction more efficient. Moreover, MBG values due to mixed phases in the compound catalyst reduce the recombination rate of the photogenerated exciton pairs leading to enhancement of photocatalytic activity. In the case of MBG SCs, the material can absorb light having different wavelengths, the energy of which corresponds to the different values of BGs. Due to this a broad range of light is absorbed which in turn generate more exciton pairs. The photogenerated electrons are transferred into the CB which is lowest in energy amongst the various phases and holes are transferred into the VB which is highest in energy amongst the various phases. This results in charge separation which consequently lowers the recombination rate of exciton pairs and provides more excitons for photocatalytic activity. The charge transfer mechanism in MBG SC is visualized in figure 4.6. The different steps of heterogeneous catalysis, as in our case, are

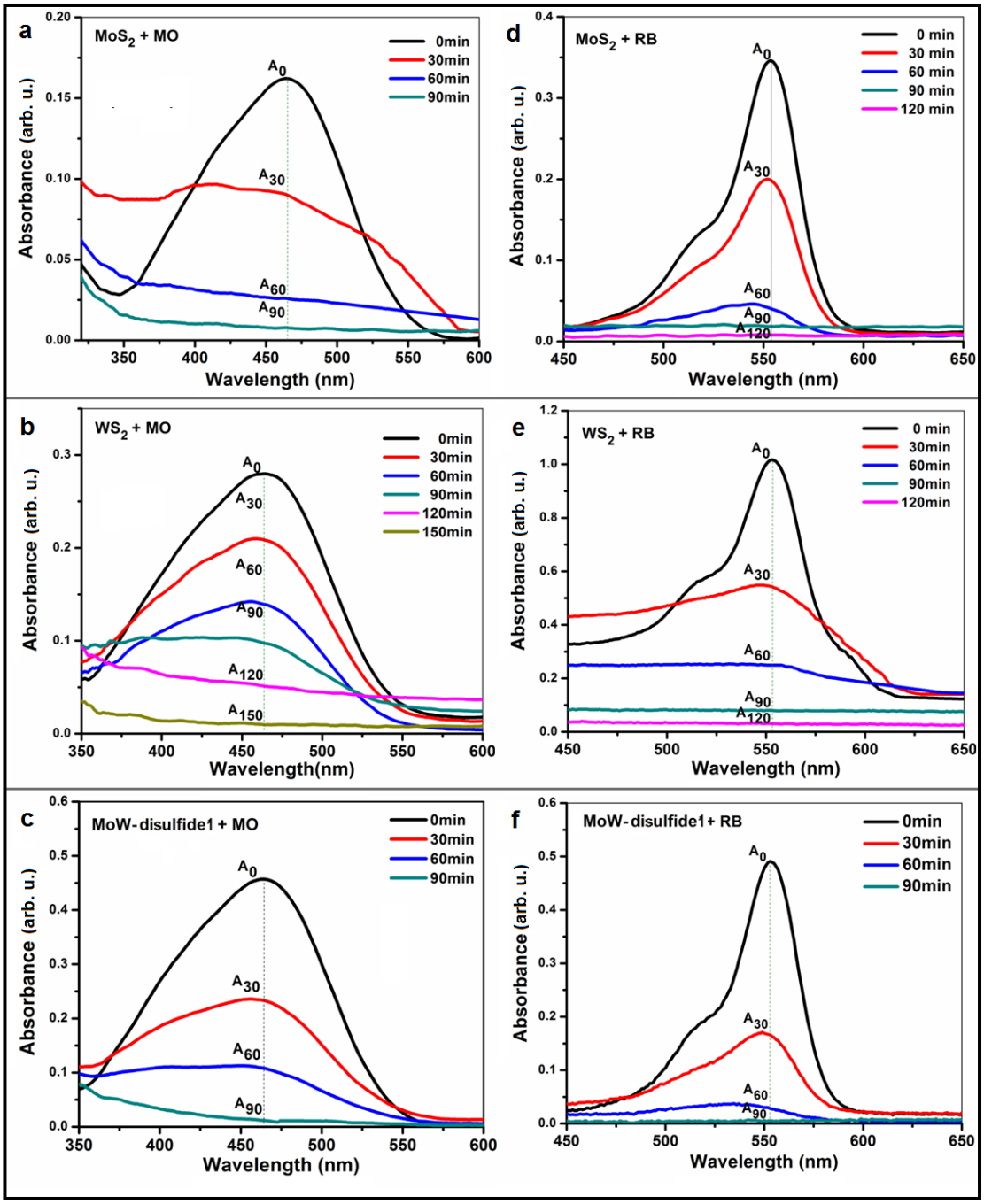

Figure 4.4 Absorption spectra of MO (a, b & c) and RB (d, e & f) degraded by MoS_2, MoW-disulfide1, and WS_2 NPs catalysts respectively under light irradiation.

explained in the following steps and visualized in figure 4.7 [8, 12-14].

Step 1: Absorption of a photon (hν) by the SC catalyst generating exciton pairs.

$$h\nu\,(\text{photon}) + \text{catalyst}\,(\text{semiconductor}) \rightarrow \text{catalyst}\,(h^+ + e^-) \qquad (h\nu \geq E_g)$$

Step 2: Oxidation and reduction processes for the generation of hyper-reactive hydroxyl free radicals and superoxide anions.

$$h^+ + H_2O \rightarrow H^+ + \bullet OH \text{ (hyper-reactive hydroxyl free radical)}$$

$$2h^+ + 2H_2O \rightarrow 2H^+ + H_2O_2$$

$$e^- + O_2 \rightarrow \bullet O_2^- \text{ (super oxide anions)}$$

$$\bullet O_2^- + 2H_2O + H^+ \rightarrow H_2O_2 + O_2$$

$$H_2O_2 \rightarrow 2 \bullet OH$$

Step 3: Degradation of reactant species (R→ MO/RB/dye) by hyper-reactive hydroxyl free radicals, superoxide anions, and photo-generated holes.

$$R + \bullet OH \rightarrow R'^{\bullet} \text{ (degraded product)} + H_2O$$

$$R + \bullet O_2^- \rightarrow R^{-\bullet} \text{ (degraded product)}$$

$$R + h^+ \rightarrow R'^{+} \text{ (degraded product)}$$

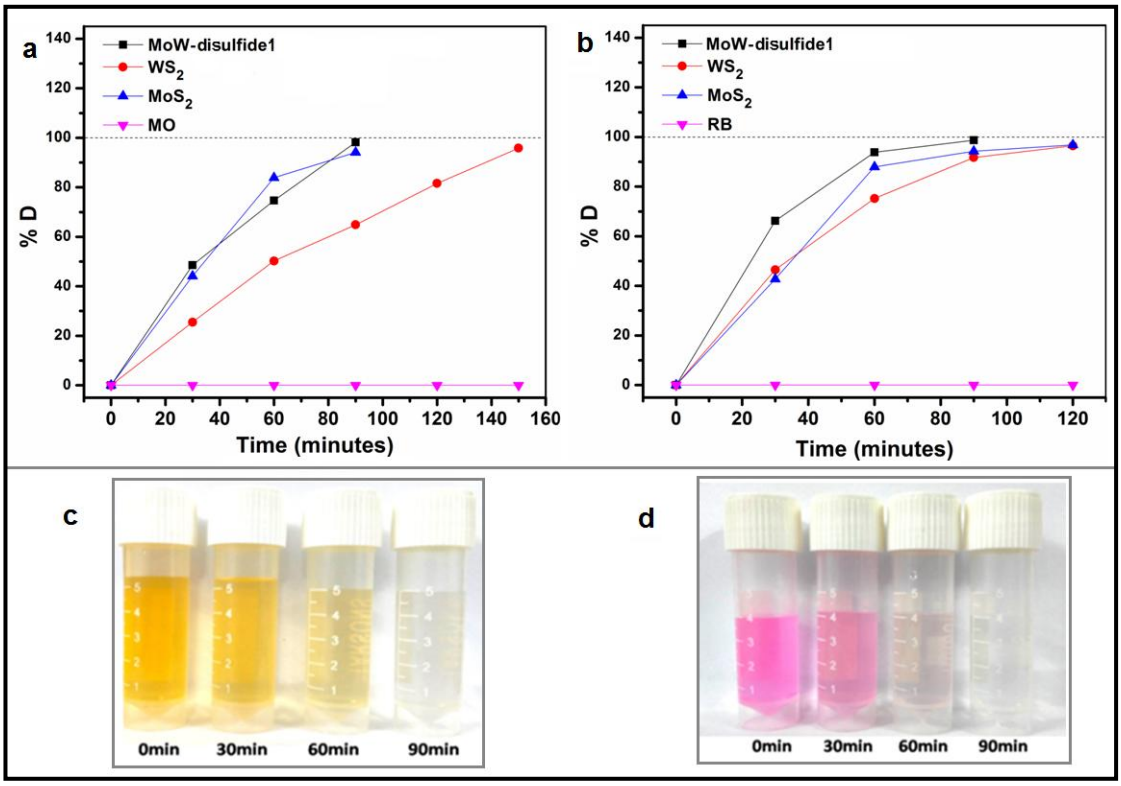

Figure 4.5 Comparison of percentage degradation measurements of (a) MO and (b) RB using all the catalysts, Decolourisation of (c) MO and (d) RB using MoW-disulfide1 photocatalyst.

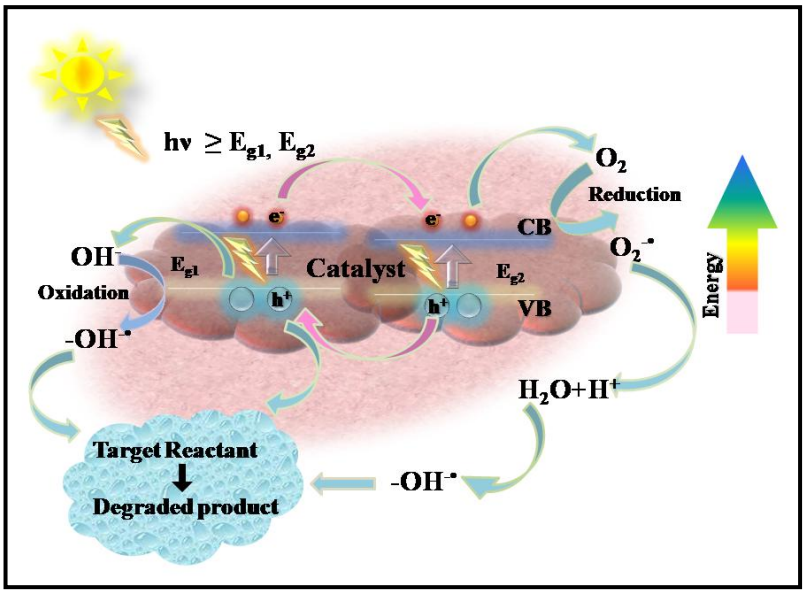

Figure 4.6 A photocatalytic mechanism for a catalyst having Multiple BGs showing transfer of electron-holes with the oxidation-reduction process.

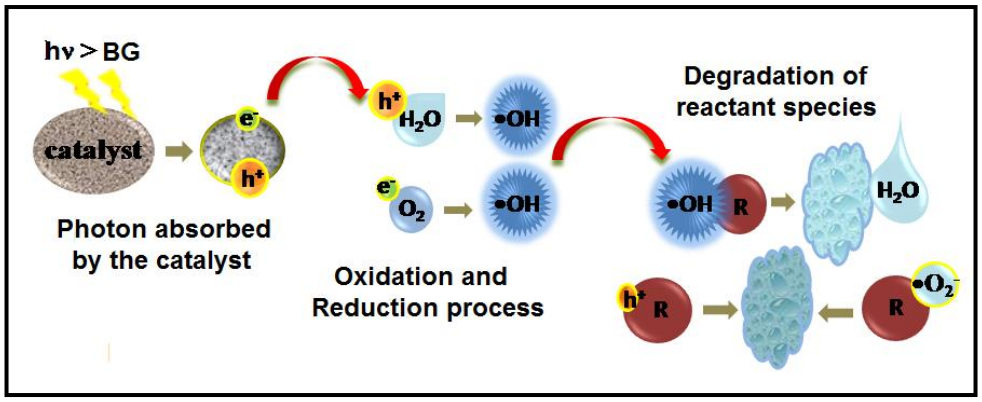

Figure 4.7 Schematic diagram showing different steps of the heterogeneous photocatalytic reaction.

4.3.2 Kinetic study of photocatalytic reactions

In order to study the kinetics of the catalytic reactions, we have employed Langmuir-Hinshelwood (L-H) mechanism [8, 15-17]. The reaction rate constant (RC) represents a measure of how fast or slow the reaction proceeds in time. In L-H mechanism the rate equation for heterogeneous catalysis is written as

$$-\frac{dC}{dt} = k_r \frac{k_{ad} C}{1 + k_{ad} C} \tag{4.2}$$

where k_r and k_{ad} are the rate constant and the adsorption coefficient respectively, C is the concentration of the dye solution. In case of highly diluted solution, i.e. C (mol/l) < 10^{-3} the $k_{ad}C$ term in the denominator of equation 4.2 can be neglected (since $k_{ad}C << 1$) and we can rewrite the equation as

$$-\frac{dC}{dt} = k_r k_{ad} C = K_r C \tag{4.3}$$

Equation 4.3 looks similar to the rate equation of a pseudo-first order reaction where K_r is the apparent RC. Applying boundary condition $C=C_0$ at t=0, and integrating equation 4.3 we get the modified rate equation as

$$\ln\left(\frac{C_0}{C_t}\right) = K_r t \tag{4.4}$$

As the reactant concentrations, in our experiments, are very low we could use equation 4.4 to determine the value of K_r. Also using the relation between absorbance and concentration of the solution (Beer-Lambert law) the concentration term in equation 4.4 can be replaced by absorbance term to obtain a similar expression 4.5. From the experimentally obtained data, the value of RC can be determined by plotting $\ln(A_0/A_t)$ vs t [8, 16].

$$\ln\left(\frac{A_0}{A_t}\right) = K_r t \tag{4.5}$$

In figure 4.8, figure 4.9 and figure 4.10, the plots for determining RC values of various catalytic reactions are shown. The experimental kinetics data are treated with three types of kinetic models namely pseudo first order, zero order and polynomial regression to investigate the mechanism of the degradation process. The %D values, RC values,

correlation coefficients (R^2) and half-life period ($t_{1/2}$) along with polynomial fitting equations are listed in table 4.3. The zero order kinetics can be explained by equation 4.6.

$$A_0 - A_t = K_r t \quad (4.6)$$

In all cases, pseudo first order and polynomial regression give a better fit than zero order regression. The linear regressions suggest that the kinetics of each reaction follows L-H pseudo first order mechanism. Also, we have observed that as the concentration of dye or catalyst changes, the reaction rate changes accordingly (graphs are not included), which suggests that the kinetics do not follow zero-order mechanism.

Table 4.3 Different parameters (%D, RC, R^2 and $t_{1/2}$) of the pseudo first order, zero order and polynomial regression for photocatalytic degradations of MO and RB using catalysts MoS_2, MoW-disulfide1, and WS_2 NPs.

Dye	Catalyst	% D (in 90 min)	Pseudo first order kinetics			Zero-order kinetics		Polynomial regression	
			RC (min^{-1})	R^2	$t_{1/2}$ (min)	RC ($M.min^{-1}$)	R^2	R^2	Polynomial equation
MO	MoS_2	94.06	0.0257	0.97	26.96	0.0015	0.90	0.94	$y=-4.96885\times10^{-5}x^2+0.03186x-0.8986$
	MoW-disulfide1	98.21	0.0381	0.92	18.19	0.00544	0.96	0.99	$y=3.39224\times10^{-4}x^2+0.00752x-0.03405$
	WS_2	64.87	0.0189	0.94	36.67	0.0019	0.98	0.96	$y=1.37511\times10^{-4}\ x^2-0.00116x-0.10439$
RB	MoS_2	94.27	0.0316	0.97	21.93	0.00343	0.93	0.96	$y=-3.83087\times10^{-5}x^2+0.03618x-0.13912$
	MoW-disulfide1	98.72	0.0493	0.99	14.06	0.0064	0.92	0.99	$y=1.35286\times10^{-4}x^2+0.03709x-0.03767$
	WS_2	91.75	0.0285	0.99	24.32	0.0097	0.95	0.99	$y=6.19038\times10^{-5}x^2+0.0211x-0.02861$

It has been observed from table 4.3 that the RC value for the catalytic reaction using the as-synthesised compound MoW-disulfide1 NPs as a catalyst is higher as compared to that using MoS_2 and WS_2 NPs as a catalyst in both the cases for MO and RB. High RC value represents increased speed of the catalytic reaction. Thus the as-synthesised compound MoW-disulfide1 NPs shows higher photocatalytic efficiency as compared to the

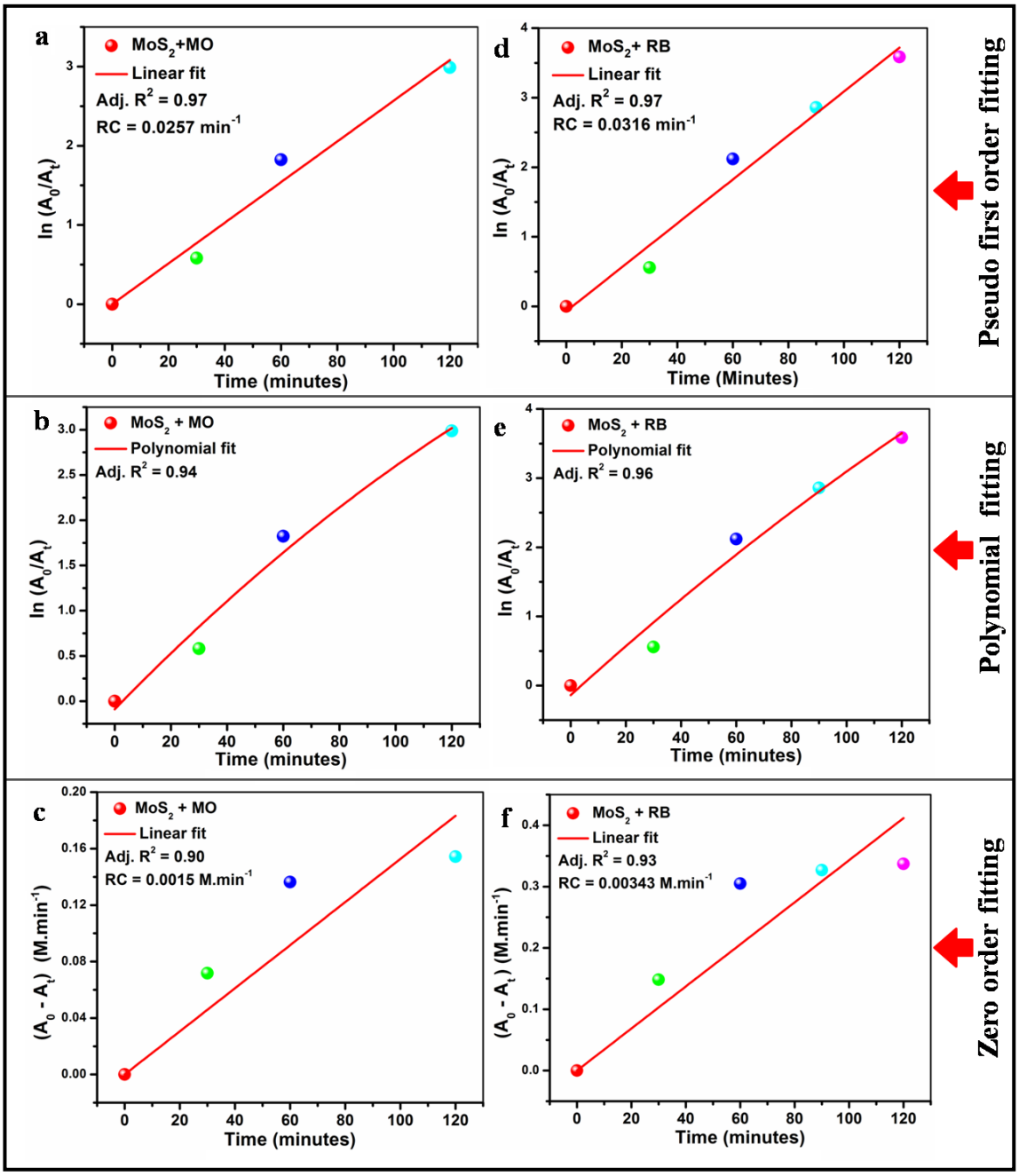

Figure 4.8 Photocatalytic degradation kinetics of MO for (a) pseudo first order, (b) polynomial and (c) zero order regression using MoS_2 NPs catalyst and of RB for (d) pseudo first order, (e) polynomial and (f) zero order regression using MoS_2 NPs catalyst.

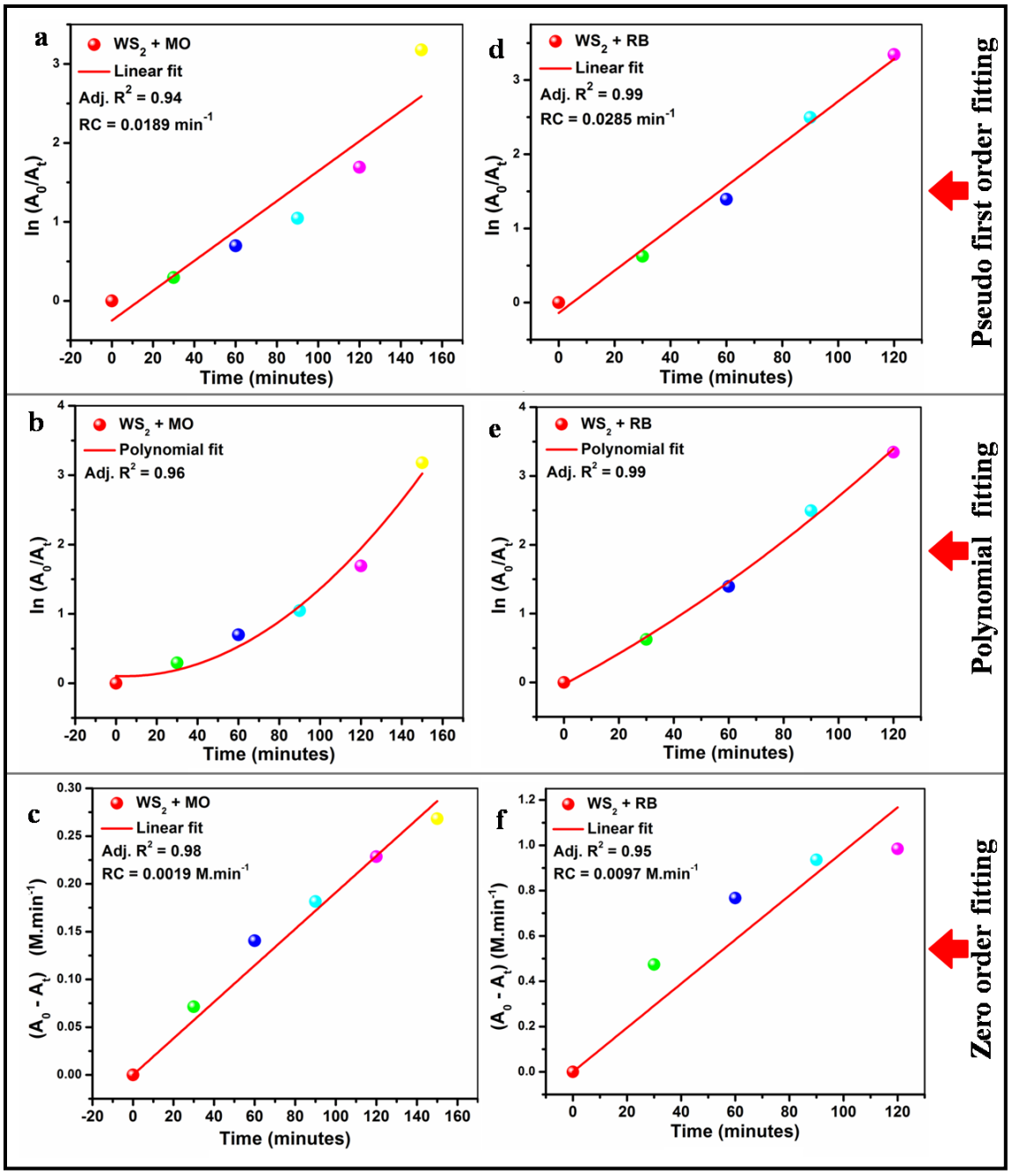

Figure 4.9 Photocatalytic degradation kinetics of MO for (a) pseudo first order, (b) polynomial and (c) zero order regression using WS_2 NPs catalyst and of RB for (d) pseudo first order, (e) polynomial and (f) zero order regression using MoS_2 NPs catalyst.

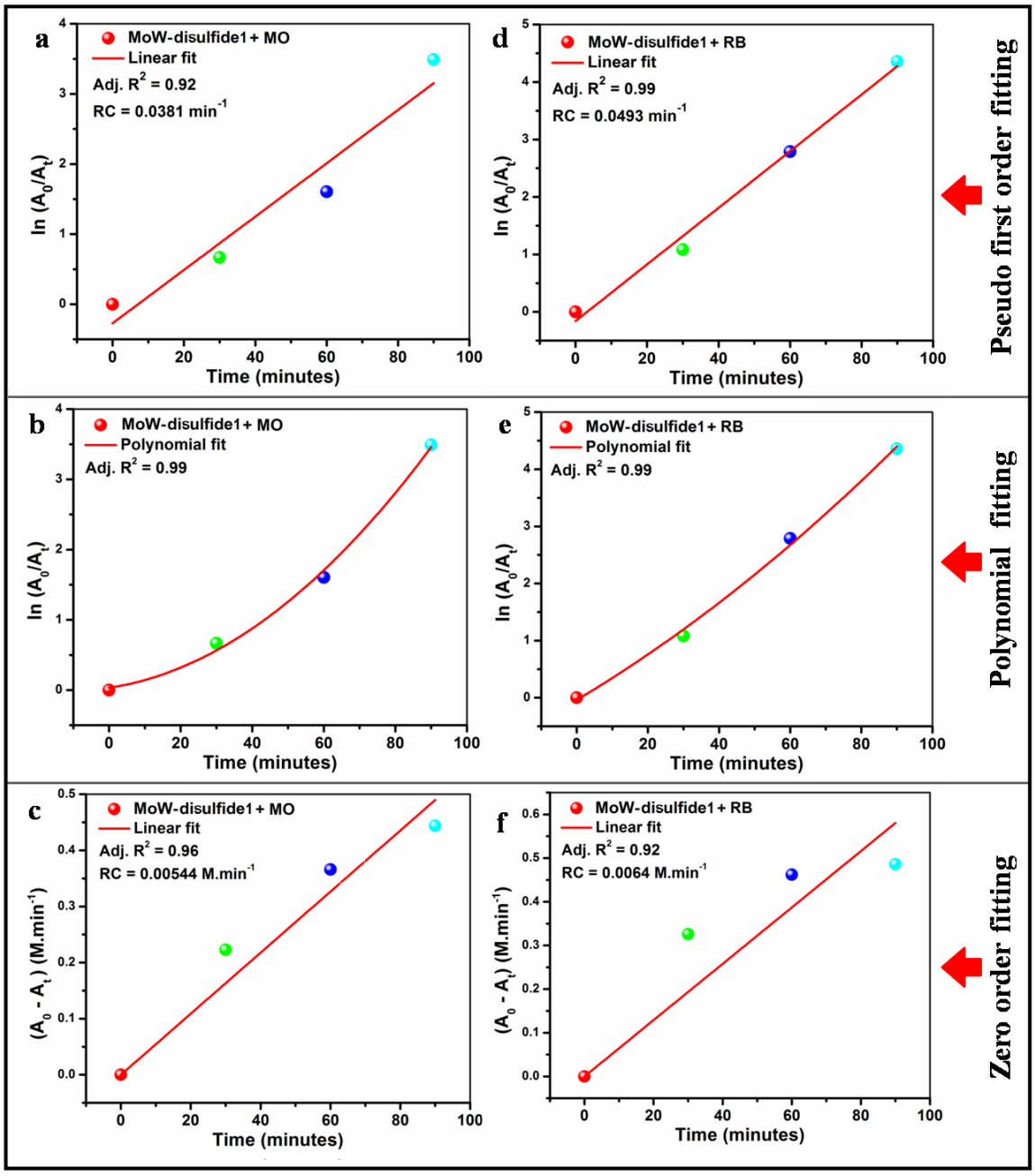

Figure 4.10 Photocatalytic degradation kinetics of MO for (a) pseudo first order, (b) polynomial and (c) zero order regression using MoW-disulfide1 NPs catalyst and of RB for (d) pseudo first order, (e) polynomial and (f) zero order regression using MoW-disulfide1 NPs catalyst.

MoS_2 and WS_2 NPs.

4.3.3 Testing reusability of the MoW-disulfide1 NPs as a catalyst

The reusability of the as-prepared compound MoW-disulfide1 catalyst is another advantageous way to make the catalytic process cost efficient. The reusability of MoW-disulfide1 NPs catalyst was tested and for this purpose, the ternary compound catalyst was extracted by centrifugation of the solution mixture after each photocatalytic treatment followed by cleaning with warm distilled water for several times and dried. The powdered catalyst was then subjected to XRD and EDX analysis after seven consecutive catalytic reactions. We observed from the EDX spectra that the composition of the as-synthesized material was not altered. Again, we have not observed any extra peaks representing any one of the dyes in the XRD pattern of the compound catalyst which is a confirmation of nonabsorbance of the dye by the catalyst. Figure 4.11 represents the EDX and XRD pattern of MoW-disulfide1 NPs catalyst after subjecting to seven consecutive photocatalytic treatments. These outcomes clearly show that the catalyst quality is not degraded and hence could be reused.

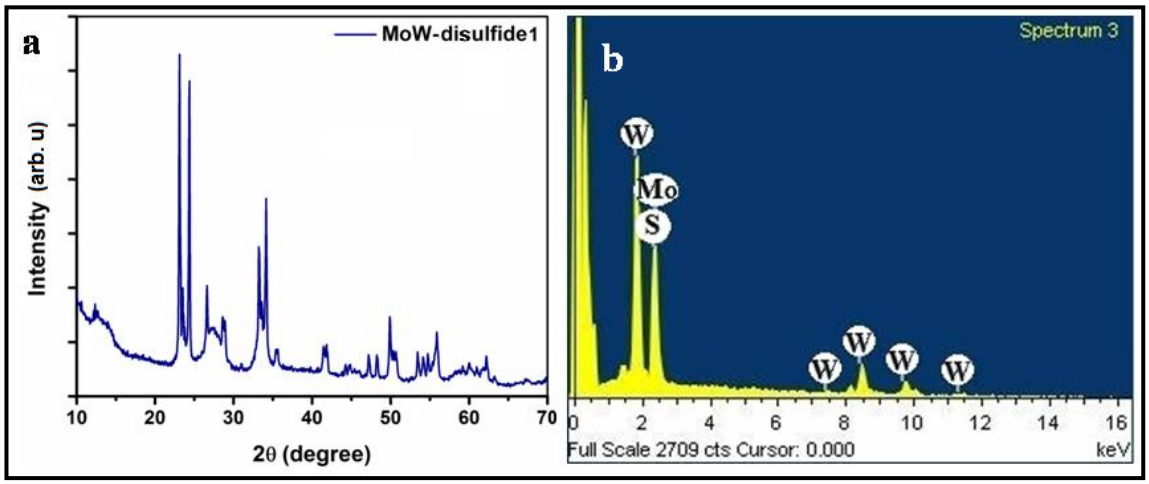

Figure 4.11 (a) XRD and (b) EDX spectra of the compound catalyst recycled after seven consecutive photocatalytic reactions. The noise below 0.5keV is not taken into consideration.

4.4 Conclusions

The synthesis of compound MoW-disulfide1 NPs along with MoS_2 and WS_2 NPs using solid-state reactions, as described in chapter 3, has been successfully achieved. Characteristic observations by using XRD, SEM, TEM, EDX, and UV-vis absorption spectroscopy depicts that compound MoW-disulfide1 NPs compound material has multiple BGs with mixed phase morphology. A comparative study of the photocatalytic activity of the as-prepared materials using MO and RB as model dyes describes that the as-synthesized compound NPs is a better photocatalyst which can utilize a broad range of solar spectra. The photodegradation mechanism follows Langmuir-Hinselwood (L-H) pseudo-first-order kinetics under experimental conditions and about 99% degradation in just 90 mins of irradiation is observed in case of ternary compound MoW-disulfide1 NP catalyst. BET and BJH analyses show that MoW-disulfide1 has the maximum surface area and larger pores as compared to the other two photocatalysts. These properties raise the photocatalytic activity of the as-prepared ternary compound material. The reusability of the compound MoW-disulfide1 catalyst makes the catalytic process a reliable and cost-effective technique. The as-synthesized compound NPs catalyst has potential applications in the field of wastewater treatment and pollution degradation.

[Note: This work is published in Journal of Envionmental Chemical Engineering.

Kalita, D., Chetia, L. and Ahmed, G. A. Synthesis of MoW-disulfide compound nanoparticles as a photocatalyst and comparison of its performance with MoS_2 and WS_2 nanoparticles. *Journal of Environmental Chemical Engineering*, 5 (4): 3161-3171, 2017. DOI:10.1016/j.jece.2017.06.020, ISSN: 2213-3437]

References

[1] Sing, K. S. W., Everett, D. H., Haul, R. A. W., Moscou, l., Pierotti, R. A., Rouquerol, J., Siemieniewska, T. Reporting physisorption data for gas/solid systems with Special Reference to the Determination of Surface Area and Porosity. *Pure & Appl. Chem*., 57(4):603-619, 1985.

[2] Kalita, D., Chetia, L., Ahmed, G. A. Synthesis of MoW-Sulfide compound nanoparticles as a photocatalyst and comparison of its performance with MoS2 and WS2 nanoparticles. *Journal of Environmental Chemical Engineering*, 5:3161-3171, 2017. DOI:10.1016/j.jece.2017.06.020

[3] Makama, A. B., Salmiaton, A., Saion, E. B., Choong, T. S. Y., and Abdullah, N. Synthesis of CdS Sensitized TiO2 Photocatalysts: Methylene Blue Adsorption and Enhanced Photocatalytic Activities. *International Journal of Photoenergy*, 2016:1-14, 2016. DOI:10.1155/2016/2947510

[4] Carvalho, A., Ribeiro, R. M., and Castro Neto, A. H. Band nesting and the optical response of two-dimensional semiconducting transition metal dichalcogenides. *PHYSICAL REVIEW B*, 88:115205, 2013. DOI:10.1103/PhysRevB.88.115205

[5] Kumar, R., Verzhbitskiy, I., and Eda, G. Strong Optical Absorption and Photocarrier Relaxation in 2-D Semiconductors. *IEEE JOURNAL OF QUANTUM ELECTRONICS*, 51(10), 2015. DOI: 10.1109/JQE.2015.2470549

[6] Nozik, A. J., Multiple exciton generation in semiconductor quantum dots. *Chemical Physics Letters*, 457:3-11, 2008. DOI:10.1016/j.cplett.2008.03.094

[7] Paul, S., Chetri, P., Choudhury, B., Ahmed, G. A., Choudhury, A. Enhanced visible light photocatalytic activity of Gadolinium doped nanocrystalline titania: An experimental and theoretical study. *Journal of Colloid and Interface Science*. 439:54-61, 2015.

[8] Chetia, L., Kalita, D., Ahmed, G. A. Enhanced photocatalytic degradation by diatom templated mixed phase titania nanostructure. *Journal of Photochemistry and Photobiology A: Chemistry*, 338:134-145 , 2017.
DOI: 10.1016/j.jphotochem.2017.01.035

[9] Zong, X., Wu, G., Yan, H., Ma, G., Shi, J., Wen, F., Wang, L., and Li, C. Photocatalytic H2 Evolution on MoS2/CdS Catalysts under Visible Light Irradiation. *J. Phys. Chem. C* 2010, *114*, 1963-1968. DOI: 10.1021/jp904350e

[10] Mao, L., Liu, J., Zhu, S., Zhang, D., Chen, Z., and Chen, C. Sonochemical fabrication of mesoporous TiO2 inside diatom frustules for photocatalyst. *Ultrasonics Sonochemistry*, 21:527-534, 2014. DOI:10.1016/j.ultsonch.2013.09.001

[11] Wen, X., Feng, Y., Huang, S., Huang, F., Cheng, Y.-B., Green, M., and Ho-Baillie, A. Defect trapping states and charge carrier recombination in organic–inorganic halide perovskites. *J. Mater. Chem. C*, 4:793-800, 2016. DOI: 10.1039/c5tc03109e

[12] Singh, N. K., Saha, S., and Pal, A. Solar light-induced photocatalytic degradation of methyl red in an aqueous suspension of commercial ZnO: a green approach. *Desalination and Water Treatment*, 53(2): 501-514, 2013. DOI: 10.1080/19443994.2013.838520

[13] Singh, N. K., Saha, S., and Pal, A. Methyl red degradation under UV illumination and catalytic action of commercial ZnO: a parametric study. *Desalination and Water Treatment*. 56(4):1066-1076, 2014. DOI: 10.1080/19443994.2014.942380

[14] Houas, A., Lachheb, H., Ksibi, M., Elaloui, E., Guillard, C., and Herrmann, J.-M. Photocatalytic degradation pathway of methylene blue in water. *Applied Catalysis B: Environmental*, 31:145-157, 2001.

[15] Kar, R., Gupta, O., Mandol, K., and Bhattacharjee, S. Performance Study on Photocatalysis of Phenol Solution in a UV Irradiated Reactor. *J. Chem. Eng. Process Technol.* 4(1), 2013. DOI:10.4172/2157-7048.1000143

[16] Sahoo, C., Gupta, A. K., and Pillai, I. M. S. Heterogeneous photocatalysis of real textile wastewater: Evaluation of reaction kinetics and characterization. *Journal of Environmental Science and Health A*, 47(13):2109-2119, 2012. DOI:10.1080/10934529.2012.695996

[17] Baxter, R. J., and Hua, P. Insight into why the Langmuir–Hinshelwood mechanism is generally preferred. *Journal of Chemical Physics*, 116(11):4379-4381, 2002. DOI:10.1063/1.1458938